A NEW SERIES OF TURBULENT STRATIFIED FLAMES: PRELIMINARY FINDINGS

M.S. Sweeney *, **S. Hochgreb***, **M.J. Dunn****, **R.S. Barlow****

marksweeney@cantab.net

*University of Cambridge, Engineering Department, Trumpington St, Cambridge, CB2 1PZ, Cambridge

**Combustion Research Facility, Sandia National Laboratories, Livermore, California 94550, USA

Abstract

Preliminary results are given for a new series of flames in a turbulent methane/air stratified swirl burner. The degree of swirl and stratification are systematically varied to generate a matrix of experimental conditions, allowing the effects of spatial gradients of equivalence ratio and swirl-induced turbulence to be investigated. The current work focuses on non-swirling flows for brevity. Two dimensional particle image velocimetry is used to provide preliminary velocity field characterization. High resolution (< 0.1 mm) scalar measurements obtained from Rayleigh/Raman/CO laser induced fluorescence (CO-LIF) line measurements allow the behaviour of key combustion species — CH_4, CO_2, CO, H_2, H_2O and O_2 — to be probed within the instantaneous flame front. Simultaneous cross-planar OH-PLIF is used to determine the orientation of the instantaneous flame normal in the scalar measurement window, allowing temperature and progress variable gradients to be angle corrected to their three dimensional values. The OH images also enable the effects of stratification and turbulence on curvature to be investigated, though such analysis is omitted due to space constraints.

The main findings are that the behaviour of the key combustions species in temperature space is well captured on the mean by unstrained laminar flame calculations regardless of the level of stratification or swirl. The agreement deteriorates when data are conditioned on the local equivalence ratio. Values for progress variable gradients and by extension thermal scalar dissipation are found to be substantially lower than laminar values, as the thickening of the flame due to turbulence dominates the effect of increased strain. These findings hold for both premixed and stratified flames. The current series of flames are proposed as an interesting if challenging set of test cases for existing and emerging turbulent flame models, and data are available on request.

Introduction

Practical combustion applications [1–5] and model combustors designed to study relevant phenomena at atmospheric pressure [6–8] typically operate in a stratified regime. This stratification may be intentional, giving acceptable flame stability in overall lean combustion. It may be due to physical design constraints, which may impose limits on the mixing length for the fuel and oxidizer. It may also occur by accident of design. There has been a significant push in the combustion research community to investigate the effect of stratification due to its practical relevance. This section will provide a brief overview of the findings in the experimental literature; a more thorough discussion is provided in [9].

The effect of stratification on low turbulence ($u'/S_L \sim \mathcal{O}(1)$), low Reynolds number lean flames has been investigated in a small number of studies. Renou *et al* [10] found that stratification increased the flame propagation rate in unsteady flame kernels. The local variation in burning velocity results in increased flame front wrinkling relative to premixed flames, with a

corresponding broadening of curvature distributions. Pasquier *et al* [11] studied the propagation of flames through stratified lean turbulent propane mixtures in a combustion bomb. The fuel concentration ahead of the flame and the local velocity indicated that flame propagation was influenced by the stoichiometry history of the mixture, whereby locally lean mixtures burn faster if pockets of richer burned mixtures are present nearby. Robin *et al* [12] studied a rod-stabilized stratified flame. Their analysis of flame thickness and curvature indicates that the presence of stratification in lean flames leads to a decrease in flame thickness, due to additional stretch components arising from differential flame propagation speeds. Anselmo-Filho *et al* [13] used a low turbulence, rod-stabilized slot burner flame, and found that curvature distributions are broadened, and that the flame surface density is increased relative to the premixed case.

A number of recent experimental studies examining results from novel turbulent stratified burners at more practically relevant turbulence levels [14–18]. Seffrin *et al* [14] introduced an axisymmetric concentric-tube burner designed to allow the investigation of flames at high Reynolds numbers ($Re \sim \mathcal{O}\left(10^4\right)$). Laser doppler velocimetry (LDV) and particle image velocimetry were used to characterize the velocity field for a number of operating conditions. The structure of these flames were investigated by Böhm *et al* [15] using Rayleigh scattering; the resulting mean and RMS profiles of temperature indicated a larger turbulent burning speed in the premixed cases relative to the corresponding stratified cases. Examining instantaneous temperature profiles and corresponding OH-PLIF images, Böhm *et al* conclude that the effect of stratification on temperature profiles is secondary to that of the actual three dimensional flame geometry. Additionally they found that curvature distributions trended similarly with stratification to those reported by Anselmo-Filho *et al* [13]. Vena *et al* [18] examined the effects of equivalence ratio gradients on the topology of flame fronts in a turbulent iso-octane/air V-flame. They observed variations in curvature distributions that were less significant than those reported elsewhere in the methane/air literature. Their main conclusion was that gradient effects on curvature may be limited in locally stoichiometric flames.

The present work presents results from a series of methane/air flames in a new turbulent swirl burner. The aim is to highlight the effects of stratification (where present) and also to demonstrate a new approach to line-imaged multiscalar measurements, which involves wavelet denoising of spatially over-sampled data.

Experimental Details The swirl burner consists of two annular channels through which fuel/oxidizer mixtures can flow, and a large air co-flow to prevent the entrainment of ambient air. The innermost annulus is terminated in a ceramic cap which acts as a central bluff body, aiding flame stabilization. Exit geometry is shown in Figure 1. A variable degree of swirl can be introduced to the outer flow by forcing a percentage of the overall outer flow through a swirl plenum which connects to the outer annulus via inclined inlet jets near the base of the burner. The development length of the burner is over 25 hydraulic diameters in both annuli to ensure fully developed turbulent flow by exit.

A matrix of operating conditions was created for experiments using the swirl burner. These conditions were chosen to allow the investigation of flames in premixed and stratified regimes, with or without swirl. Bulk velocities were chosen to maximize the Reynolds numbers in the flows given the physical constraints imposed by the mass flow controllers available and the maximum throughput of the laboratory air supply.

The bulk velocity in the outer annulus, U_{o} = 18.7 m/s, was nominally held at approximately twice the value of the velocity in the inner annulus, U_{i} = 8.31 m/s, in order to generate substantial levels of shear between the two flows and ensure thorough mixing of the flows near to the burner mouth. Co-flow air was supplied around the outer annulus with a bulk velocity $U_{\mathrm{co-flow}}$ = 0.4

Figure 1. Plan and end view of swirl burner exit geometry. All dimensions are in mm and are drawn to scale.

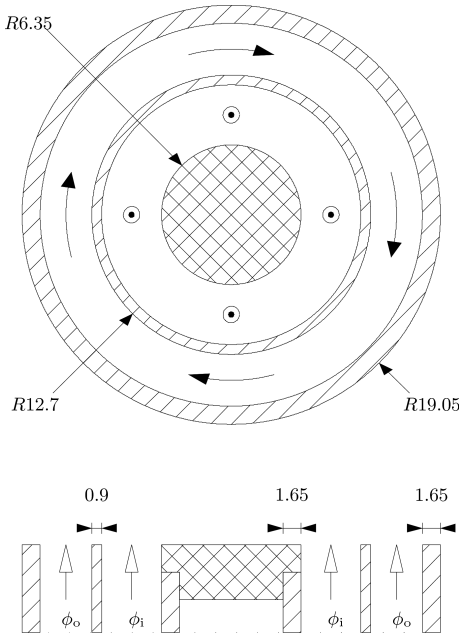

m/s to prevent the entrainment of ambient air.

The stratification ratio was varied from 1 for premixed cases to 3 for highly stratified cases. The swirl ratio was varied between 0 for purely axial flow to 0.4 for highly swirling flow. Gas flows in all experiments were metered using mass flow controllers. These conditions are listed in full in Table 1. The swirl fraction is the fractional split of the total volumetric flow to the outer annulus between the axial flow plenum and the tangential swirl plenum. $SwB4$, $SwB8$, $SwB12$, and $SwB16$ are omitted as it was not possible to stabilize the highly stratified cases at this high swirl fraction (0.4). In the interests of brevity only the lean non-swirling cases ($SwB1$, $SwB5$, and $SwB9$) are considered in the present work.

Table 1. Operating conditions for Cambridge Stratified Swirl Burner. In all cases U_i is $8.31\,\mathrm{m\,s^{-1}}$ and U_o is $18.7\,\mathrm{m\,s^{-1}}$, and the $U_\mathrm{co-flow}$ is $0.4\,\mathrm{m\,s^{-1}}$

Flame	Swirl Fraction	$\phi_\mathrm{i}/\phi_\mathrm{o}$	ϕ_i	ϕ_o	ϕ_g
$SwB1$	0.0				
$SwB2$	0.25	1	0.75	0.75	
$SwB3$	0.33				
$SwB5$	0.0				
$SwB6$	0.25	2	1.0	0.5	
$SwB7$	0.33				0.75
$SwB9$	0.0				
$SwB10$	0.25	3	1.125	0.375	
$SwB11$	0.33				
$SwB13$	0.0				
$SwB14$	0.25	1	1.0	1	1
$SwB15$	0.33				

Multiscalar laser diagnostics were applied at the Turbulent Combustion Laboratory in Sandia National Laboratories. The diagnostics setup allows for the line measurement of temperature (Rayleigh scattering) and major species (Raman scattering) with simultaneous cross planar OH-PLIF. The experimental setup is illustrated in Figure 2. This setup has previously been described in [19–21]. Beams from four frequency doubled Nd:YAG lasers were used for Raman and Rayleigh line imaging, yielding a total energy of 1.8 J/pulse in the probe volume. The focus had a diameter of 0.22 mm ($1/e^2$). The beam diameter was 0.24 mm at the ends of the 6 mm length of the measured segment. CO was excited at 230.1 nm (two photons), with the UV laser beam aligned on the same axis as the Nd:YAG laser beams. The line measurement window of 6.18 mm at a pixel resolution of 0.02 mm. This high resolution is achieved by oversampling the data and then applying wavelet denoising; details on this technique will be published in [22]. The effective spatial resolution of the measurements is roughly $100\,\mu$m and is limited by the optical resolution of the imaging system, the laser beam diameter, and blurring effect of the flame itself, which is difficult to evaluate. Signal to noise ratios for measurements in the current experiment are detailed in Table 2.

Simultaneous cross-plane images of OH-LIF were also taken to allow the determination of the local flame orientation (3D normal vector) and the flame-normal gradient of the reaction progress variable. The LIF investigation windows were 8.06 mm wide by 4.03 mm tall at a resolution of 0.048 mm/pixel, centered along the line measurement axis, and oriented at 32° to the vertical.

Preliminary velocity characterization was carried out using particle image velocimetry (PIV). The inner annulus, outer annulus, and co-flow were each seeded with $1\,\mu$m calcined aluminium oxide particles. These particles were illuminated using a double-pulsed Nd:YaG laser (Litron NanoIV) operating at 532 nm. Each pulse was separated by a Δt of $16\,\mu$s. The light scattered by the seed particles was imaged using a CCD camera (LaVision Imager Pro X 4M) fitted with a Nikon AF Micro Nikkor 60 mm lens (f/4) and a 50 mm interference filter centered about 532 nm (0.5 nm FWHM). The images were $69.3\,$mm wide by $69.3\,$mm tall, with a resolution of $34.1\,\mu$m. Vectors were calculated using single-pass cross-correlation with a 32×32 window size and 50% overlap, giving a resolution of 0.55 mm/vector.

Data Processing

Local mixture fraction is calculated from the line measurement data using the Bilger formula-

Table 2. Signal to noise (SNR) ratios in scalar measurements in SwB based on measurements in the products of a CH_4/air flat calibration flame ($T = 2050\,$K, $\phi = 1.28$), for both the $100\,\mu$m resolution data and the wavelet denoised data, arranged in order of decreasing SNR.

Scalar	$100\,\mu$m Data	Wavelet Denoised Data
T	150	200
Y_{N_2}	130	190
Y_{H_2O}	50	88
ϕ	65	86
Y_{CO_2}	29	45
Y_{CO}	16	23
Y_{H_2}	17	24

Figure 2. Illustration of multiscalar laser diagnostic setup in the Turbulent Combustion Laboratory in Sandia National Laboratories.

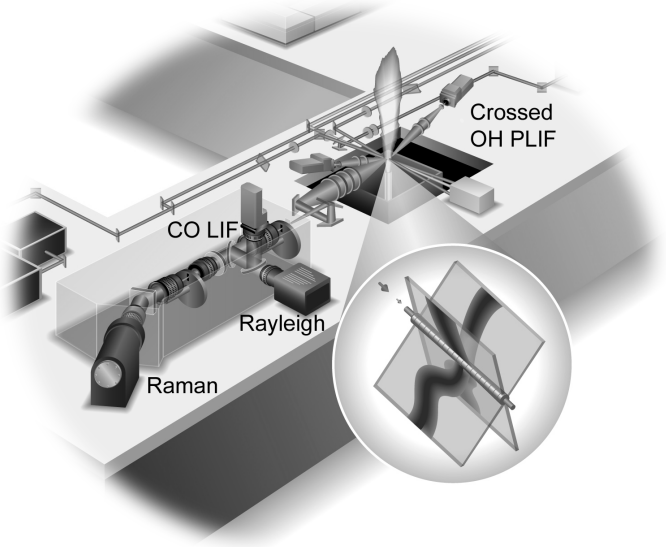

tion [23] and the major combustion species:

$$Z = \frac{2Y_{\mathrm{C}}/M_{\mathrm{C}} + 0.5Y_{\mathrm{H}}/M_{\mathrm{H}} + (Y_{\mathrm{O},2} - Y_{\mathrm{O}})/M_{\mathrm{O}}}{2Y_{\mathrm{C},1}/M_{\mathrm{C}} + 0.5Y_{\mathrm{H},1}/M_{\mathrm{H}} + Y_{\mathrm{O},2}/M_{\mathrm{O}}} \tag{1}$$

where Y_{a} is the mass fraction of the sum of all measured species containing the element a, M_a is the atomic weight of element a, and the subscripts 1 and 2 refers to values in fuel and air respectively.This definition allows the mixture fraction to be approximately conserved across the reaction zone. A corresponding equivalence ratio ϕ is derived from this definition to coincide with the usual definition of ϕ in the fresh mixture:

$$\phi(Z) = \frac{Z}{1-Z}\frac{1-Z_{\mathrm{s}}}{Z_{\mathrm{s}}} \tag{2}$$

where Z_{s} is the stoichiometric mixture fraction. The present work makes use of a thermal progress variable, $c(T,\phi)$, which is dependent on both the local temperature and stoichiometry, enabling its application to stratified cases. The formula for this is as follows:

$$c_{\mathrm{T}}(x,\phi) = \frac{T(x) - T_{\mathrm{u}}}{T_{\mathrm{e}}(\phi) - T_{\mathrm{u}}} \tag{3}$$

where $T(x)$ is the local temperature, T_{u} is the temperature in the unburned reactants, and $T_{\mathrm{e}}(\phi)$ is the equilibrium flame temperature as a function of ϕ (determined from premixed unstrained laminar flame calculations[1]).

Scalar gradients are angle corrected to their three dimensional values using the cosine of the solid angle between the line measurement axis and the three dimensional flame normal. The flame normal is obtained from the cross-planar OH-PLIF images, using the methods described in Karpetis *et al* [19, 20]. As noted by Karpetis *et al*, the accuracy of angle correction decreases with increasing solid angle; in the current experiments, records with solid angles greater than

[1]Laminar flame calculations were generated using CHEMKIN [24] and GRI-Mech 3.0 [25]

50° were discarded to minimize inaccuracies.

Results and Discussion

Results are presented as follows: non-reacting velocity profiles at $z = 5\,\text{mm}$; sample instantaneous profiles of T and ϕ; Favre averages; conditional mean fits of major species in temperature state-space; conditional mean fits of surface density function and scalar dissipation in progress variable space. All data was taken at the intersection of the mixing layer and the mean flame brush (located at $z = 30\,\text{mm}$/$z = 50\,\text{mm}$/$z = 50\,\text{mm}$ for the $SwB1$/$SwB5$/$SwB9$ cases respectively). The premixed dataset was 5000 records long, while the stratified sets contained $30\,000$ records to allow for data reduction when conditioning on equivalence ratio.

Figure 3. *Left*: Exit velocities and fluctuations in non-reacting case at $z = 5\,\text{mm}$. Mean/fluctuating velocities shown solid/dotted lines lines. Axial components denoted by open triangles, while radial components are marked by open circles. *Right*: Borghi diagram of reacting cases. $SwB1$, $SwB5$ and $SwB9$ are shown by open triangle, circle and square markers.

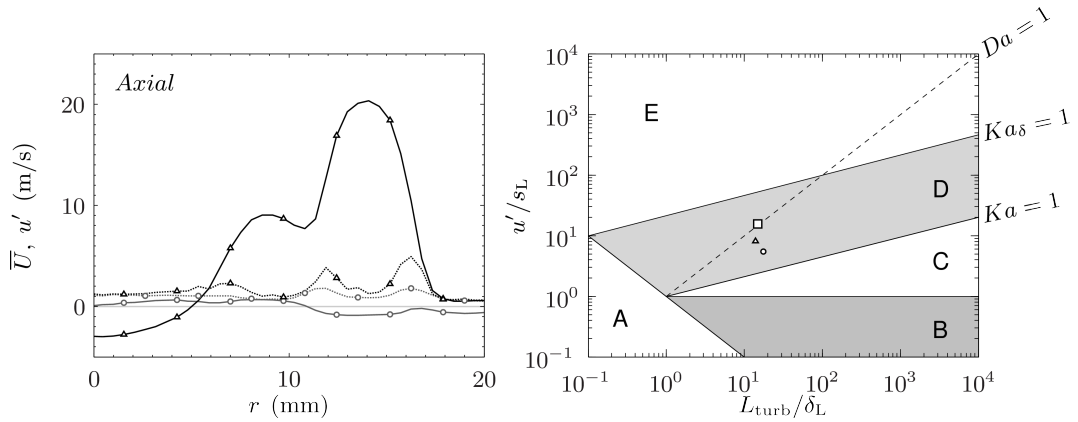

The mean and rms velocity profiles near exit ($z = 5\,\text{mm}$) are shown for non-reacting, non-swirling flow in Figure 3, corresponding to $SwB1$, $SwB5$, $SwB9$ and $SwB13$. The exit profiles demonstrate behavior consistent with fully developed channel flow, with peaks in $\overline{U}_\text{z}$ corresponding to flow from the inner and outer annuli. The peak due to the latter is approximately twice that of the inner flow, as expected from the nominal bulk velocities calculated for the annuli. $\overline{U}_\text{z}$ is negative for $r < 5\,\text{mm}$, corresponding to a recirculation zone above the burner's ceramic cap, which acts as a central bluff body. The extent and strength of the turbulent mixing layers between the inner- and outer-flows and the outer-flow and the co-flow air are shown by u'_z. The measured radial velocity $\overline{U}_\text{r}$ is almost negligible in comparison to the axial velocity this close to the exit. The radial fluctuations u'_r are similar to their axial counterpart, showing peaks in the shear layers between the inner- and outer-flows and also the outer- and co-flow. Turbulence parameters calculated at the intersection of the mixing layer and the mean flame brush are shown in Table 3, and it is clear that the flames surveyed lie in the thin reaction zone regime on the modified Borghi diagram (Figure 3).

In the interests of brevity, instantaneous data presented is limited to temperature and equivalence ratio. Figure 4 shows instantaneous profiles of temperature and equivalence ratio in the axial swirl burner cases, using data taken from the intersection of the mixing layer and the mean flame brush. The T data for $SwB1$ are plotted with black dots at each point to demonstrate the resolution of the wavelet filtered data; the pixel resolution is sufficiently fine that individual

Table 3. Key turbulence parameters for $SwB1$, $SwB5$ and $SwB9$ at the intersection of the mixing layer and the mean flame brush.

Flame	$\overline{U}$ ($\mathrm{m\,s^{-1}}$)	u' ($\mathrm{m\,s^{-1}}$)	I (%)	$\mathrm{Re_t}$	L_{turb} (mm)	η_{K} (µm)	τ_{K} (µs)	ν_{K} ($\mathrm{m\,s^{-1}}$)	Da	Ka
$SwB1$	10.36	1.16	11	172	10	210	655	0.3	3.0	11.2
$SwB5$	14.83	3.95	27	494	10	95	114	0.8	0.9	34.7
$SwB9$	13.67	4.84	35	483	10	97	94	1.0	0.6	62.3

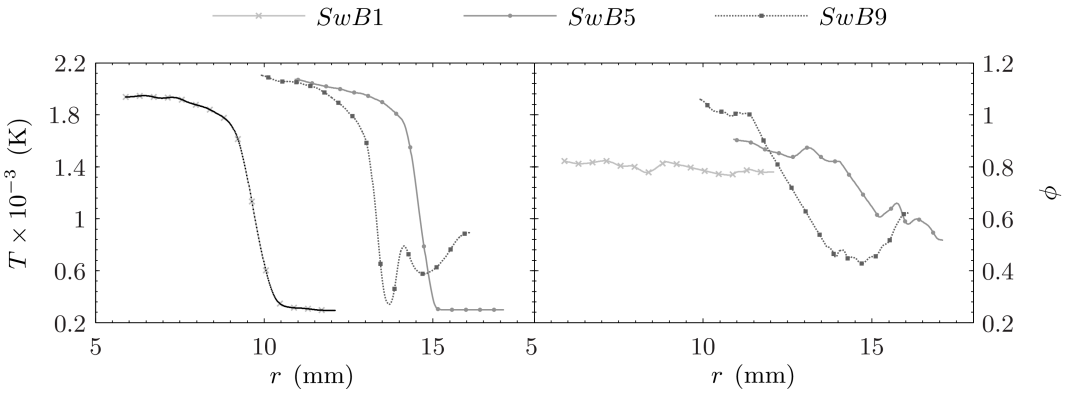

Figure 4. Single-shot profiles of temperature and equivalence ratio at the intersection of the mixing layer and the mean flame brush, randomly selected from the $SwB1$, $SwB5$ and $SwB9$ datasets.

markers are almost indistinguishable except where gradients are large. Significant gradients in equivalence ratio are seen for both levels of stratification.

Favre averages of key combustion species are given in Figure 5, demonstrating structural differences brought about due to stratification of the inlet flows. The stratified flame brushes are shifted radially outwards relative to that for $SwB1$ due to the combined effects of higher flame speed and density change in the products. Both of these effects are attributable to the higher levels of $\widetilde{\phi}$ burned through further upstream. The stratified cases achieve higher temperature in the equilibrium zone for similar reasons. Interestingly the highly stratified $SwB9$ case stabilizes inside the $SwB5$ case, despite being at the same downstream distance ($z = 50\,\mathrm{mm}$) and having higher peak equivalence ratio. Near the burner exit the equivalence ratio experienced by $SwB9$ was found to be higher than that seen by $SwB5$ (above stoichiometric in both cases). As such the resulting local turbulent burning velocity is lower in $SwB9$ than $SwB5$, contributing to the discrepancy seen further downstream.

The plots of $\widetilde{\phi}$ show large mean gradients of equivalence ratio in the stratified cases. Interestingly, $\widetilde{\phi}$ for the premixed $SwB1$ appear elevated in the central region. This is attributed to the effect of the central recirculation zone on the hydrogen-carbon balance upstream of the measurement location. This behaviour is examined in more detail in a forthcoming publication by Barlow *et al* [26].

The Favre-averaged profiles of CO_2, O_2 and H_2O trend similarly to $\widetilde{T}$ (mirrored in the case of O_2), as is expected. Some notable behavior is observed in these species however. It is clear that in the stratified cases all oxygen is used up in reactions in the equilibrium zone, in marked contrast to the behavior in the premixed case. This is attributed to a combination of higher $\widetilde{T}$

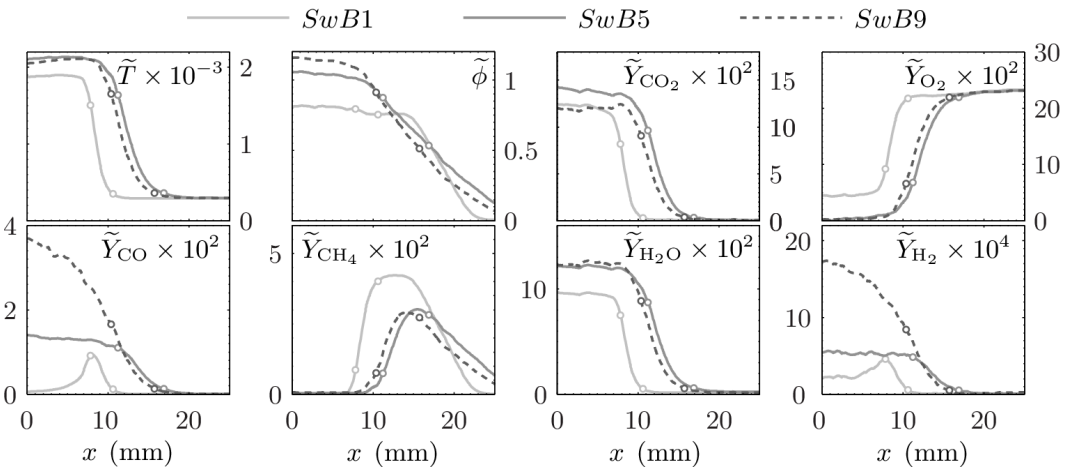

Figure 5. Radial profiles of Favre-averaged measurements, with FWHM T'' locations plotted as open circles to mark the flame brush. Favre-averaged temperature is in K.

and $\widetilde{\phi}$ and high residence time due to the recirculation zone; within the actual flame brush at the long record locations where $\widetilde{T}$ and $\widetilde{\phi}$ are similar, the behavior of $\widetilde{Y}_{O_2}$ exhibited by all three cases is very similar. The higher levels of H_2 seen in the post-flame region for the stratified cases relative to the premixed are attributed to the high equivalence ratio ($\phi > 1$) experienced further upstream, and a lack of O_2 to further increase Y_{H_2O} after the reaction zone. The peak value of $\widetilde{Y}_{CO_2}$ attained in the premixed case is similar to the $SwB9$ value, and both are attenuated relative to the moderately stratified case. The reasons for this are unclear but may be due to differential diffusion effects further upstream.

There is a sharp ramp in the level of CO through the premixed $SwB1$ flame brush, followed by a rapid decrease. In contrast, the moderately stratified case shows a gentle increase towards the centerline of the burner, which $SwB9$ increases substantially in the post-flame region. These trends track the stoichiometry of the products. $\widetilde{Y}_{H_2}$ trends similarly to $\widetilde{Y}_{CO}$. $\widetilde{Y}_{CH_4}$ trends with $\widetilde{\phi}$ in the pre-flame region before dropping to zero through the flame.

Figure 6 shows mean species mass fractions against temperature conditioned on local equivalence ratio to within $\pm 1\,\%$ of the mean $\phi = 0.79$. Y_{CO_2} is slightly elevated compared to unstrained laminar calculations, and shows negligible stratification dependence. The maximum differences are seen for the premixed case, which is $8\,\%$ greater than the laminar value in the middle of the thermal profile. The Y_{CO} calculations capture the behavior of the conditioned $SwB1$ data very well. Stratification seems to have varying influence on the Y_{CO} profiles, with $SwB5$ trending above the premixed values, and the highly stratified $SwB9$ case showing a reduced peak Y_{CO} ($-12\,\%$).

The Y_{H_2} profiles show the largest deviations from calculations. $SwB1$ is in moderate agreement, but both levels of stratification exhibit markedly different behavior in the reaction zone; whereas the calculated Y_{H_2} increases at a constant rate with increasing temperature in this region, the stratified cases show an elevated profile that is close to symmetric about the $T = 1200\,\mathrm{K}$ point. As these data are conditioned to be at the same stoichiometry as the premixed case it is unclear as to whether the differences seen in hydrogen production are due to the higher equivalence ratios in the products away from the points considered or not. Further investigation to ascertain the cause of these discrepancies is merited. Y_{O_2} and Y_{H_2O} are insensitive to the degree of stratification, and show excellent agreement with laminar flame calculations.

Figure 7 shows the behavior of $|\nabla c|$ and χ_c in progress variable space when data is con-

Figure 6. State space plots of major combustion species in $SwB1$, $SwB5$, and $SwB9$, conditioned on local equivalence ratio to within $\pm 1\,\%$ of the mean $\phi = 0.79$. Unstrained premixed laminar flame calculations are shown by solid black lines. Vertical bars indicate $\pm$ one standard deviation.

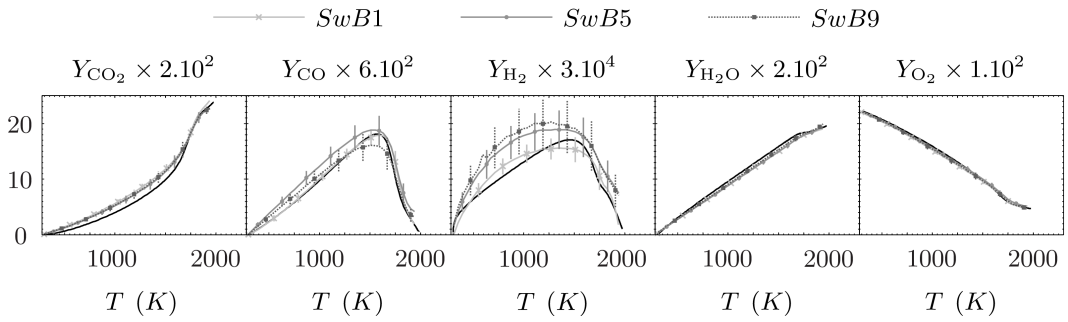

ditioned such that the local equivalence ratio is within $\pm 1\,\%$ of the mean equivalence ratio as before. This ensures that any trends observed are unlikely to be influenced unduly by stoichiometry effects. Profiles of $|\nabla c|$ trend below their laminar unstrained calculated equivalents, with the latter lying approximately one standard deviation above the experimental conditional means.

Given the degree of variance seen within the experimental data it is difficult to know whether differences seen between the means are significant. However it does appear that the premixed $SwB1$ case shows more aggressive gradients through the pre-heat and much of the reaction zone ($c < 0.5$), with the result that the surface density function peaks closer to the products for the stratified cases. The peak amplitudes are similar throughout however. The scalar dissipation shows a more convincing trend with increasing stratification, with the premixed lean case undershooting the peak stratified levels by $16\,\%$ to $20\,\%$. Interestingly the locations of peak χ_c are less sensitive to the degree of stratification than for the surface density function. In all cases the peaks attained by both $|\nabla c|$ and χ_c are substantially lower than the laminar calculations. This may be due to small turbulent eddies penetrating the pre-heat zone, resulting in a thickening of the flame front.

Conclusions

Figure 7. Mean fits of surface density function and scalar dissipation in progress variable space, conditioned on local equivalence ratio to within $\pm 1\,\%$ of the mean $\phi = 0.79$. Unstrained premixed laminar flame calculations are shown by solid black lines. Vertical bars indicate $\pm$ one standard deviation.

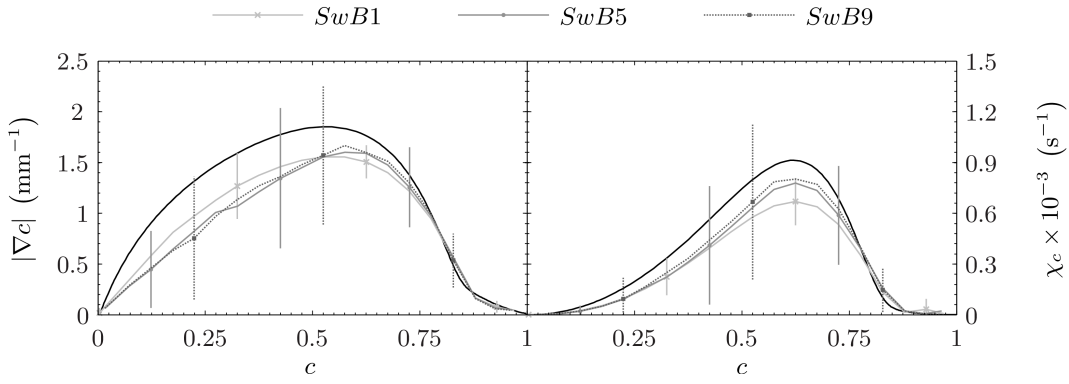

Results from a new turbulent swirling stratified methane/air burner have been presented for a subset of axial flow conditions. An experimental matrix encompassing three degrees of stratification was investigated using a variety of techniques. Axial and radial flow fields were revealed using two dimensional PIV, while the thermo-chemical structure was probed within the flame front using high resolution Rayleigh/Raman/CO-LIF line measurements with simultaneous cross-planar OH-LIF. The main results of these analyses are summarized as follows:

- The flames surveyed fall within the thin reaction zone regime on the modified Borghi diagram.
- The flames surveyed feature large recirculation zones above the central bluff body, which has significant impact on the species concentrations within the flame.
- Significant levels of stratification are achieved within the flame front.
- Favre averaged results reveal elevated equivalence ratio levels within the recirculation zone for the premixed case, which is attributed to the effects of preferential molecular transport of hydrogen away from the flame front near to the burner exit.
- The mean behavior of H_2O and O_2 in the swirl burner flames at the intersection of the mixing layer with the flame brush is well captured by the use of ensembles of unstrained laminar flame calculations. Significant differences are seen in H_2, CO, and to a lesser extent CO_2. Whether these are due solely to stratification or partially due to the effects of preferential molecular transport caused by the recirculation zone above the central bluff body could be investigated using a piloted version of the current burner.
- When conditioned on local equivalence ratio H_2 in the lean premixed cases is moderately well modeled by laminar unstrained calculations but the stratified conditions are underpredicted through much of the temperature space.
- Surface density function and scalar dissipation are significantly attenuated relative to their corresponding laminar unstrained values. The peak surface density function values are similar between stratified and premixed cases when conditioned on local equivalence ratio, but are shifted towards the products under stratified conditions. Scalar dissipation is enhanced by stratification.

Future work on this burner will focus on extending the analyses highlighted in the current study to the swirling and stoichiometric cases, which were omitted from here in the interests of brevity. The geometric structure of the flame and the influence of stratification therein will also be investigated; curvature and flame surface density will be examined and also used to condition scalar data. A campaign of stereo PIV is planned to extend the velocity characterization into three dimensions to satisfactorily capture the flow field in the swirling cases. The authors believe the current burner to be an interesting case for numerical simulations, particularly due to the effects of the recirculation zone above the central bluff body, and the data is freely available to any interested party for model validation.

Acknowledgements
The authors would like to thank the EPSRC and Rolls Royce for their financial contributions to this work, and to The Leverhulme Trust for an International Network Grant. Work at Sandia was supported by the United States Department of Energy, Office of Basic Energy Sciences, Division of Chemical Sciences, Geosciences and Biosciences. Sandia National Laboratories is

a multiprogram laboratory operated by Sandia Corporation, a Lockheed Martin Company, for the United States Department of Energy under contract DE-AC04-94-AL85000. The authors also thank Guanghua Wang and Bob Harmon for their contributions to the experiments.

References

[1] A. Mansour. Gas turbine fuel injection technology. *Proc. ASME Turbo Expo*, 2:141–149, 2005.

[2] D.A. Nickolaus, D.S. Crocker, D.L. Black, and C.E. Smith. Development of a lean direct fuel injector for low emission aero gas turbines. *Int. Gas Turbine Initiative*, 2002.

[3] H. J. Bauer. New low emission strategies and combustor designs for civil aeroengine applications. *Prog. Comput. Fluid Dyn.*, 4(3-5):130–142, 2004.

[4] A. C. Alkidas. Combustion advancements in gasoline engines. *Energy Convs. Manage.*, 48(11):2751–2761, 2007.

[5] M. C. Drake and D. C. Haworth. Advanced gasoline engine development using optical diagnostics and numerical modeling. *Proc. Comb. Inst*, 31:99–124, 2007.

[6] W. Meier, P. Weigand, X. R. Duan, and R. Giezendanner-Thoben. Detailed characterization of the dynamics of thermoacoustic pulsations in a lean premixed swirl flame. *Comb. Flame*, 150(1-2):2–26, 2007.

[7] A. X. Sengissen, J. F. Van Kampen, R. A. Huls, G. G. M. Stoffels, J. B. W. Kok, and T. J. Poinsot. Les and experimental studies of cold and reacting flow in a swirled partially premixed burner with and without fuel modulation. *Comb. Flame*, 150(1-2):40–53, 2007.

[8] C. Duwig and C. Fureby. Large eddy simulation of unsteady lean stratified premixed combustion. *Comb. Flame*, 151(1-2):85–103, 2007.

[9] M.S. Sweeney, S. Hochgreb, and R.S. Barlow. The Structure of Premixed and Stratified Low Turbulence Flames. *Comb. Flame*, 2011. doi: DOI:10.1016/j.combustflame.2011.02.007.

[10] B. Renou, E. Samson, and A. Boukhalfa. An experimental study of freely propagating turbulent propane/air flames in stratified inhomogeneous mixtures. *Comb. Sci. Technol.*, 176:1867–1890, 2004.

[11] N. Pasquier, B. Lecordier, M. Trinite, and A. Cessou. An experimental investigation of flame propagation through a turbulent stratified mixture. *Proc. Comb. Inst*, 31(1):1567–1574, 2007.

[12] V. Robin, A. Mura, M. Champion, O. Degardin, B. Renou, and M. Boukhalfa. Experimental and numerical analysis of stratified turbulent v-shaped flames. *Comb. Flame*, 153 (1–2):288–315, 2008.

[13] P. Anselmo-Filho, S. Hochgreb, R.S. Barlow, and R.S. Cant. Experimental measurements of geometric properties of turbulent stratified flames. *Proc. Comb. Inst*, 32(2):1763 – 1770, 2009.

[14] F. Seffrin, F. Fuest, D. Geyer, and A. Dreizler. Flow field studies of a new series of turbulent premixed stratified flames. *Comb. Flame*, 157(2):384 – 396, 2010.

[15] B. Böhm, J.H. Frank, and A. Dreizler. Temperature and mixing field measurements in stratified lean premixed turbulent flames. *Proc. of the Comb. Inst.*, In Press, Corrected Proof, 2010. ISSN 1540-7489.

[16] M.S. Sweeney, S. Hochgreb, M.J. Dunn, and R.S. Barlow. A comparative analysis of flame surface density metrics in premixed and stratified flames. *Proc. Comb. Inst*, 32, 2010.

[17] C. Galizzi and D. Escudié. Experimental analysis of an oblique turbulent flame front propagating in a stratified flow. *Comb. Flame*, 157(12):2277 – 2285, 2010.

[18] P.C. Vena, B. Deschamps, G.J. Smallwood, and M.R. Johnson. Equivalence ratio gradient effects on flame front topology in a stratified iso-octane/air turbulent v-flame. *Proc. Comb. Inst.*, 33(1):1551–1558, 2011.

[19] A. N. Karpetis, T. B. Settersten, R. W. Schefer, and R. S. Barlow. Laser imaging system for determination of three-dimensional scalar gradients in turbulent flames. *Opt. Lett.*, 29 (4):355–357, 2004.

[20] A. N. Karpetis and R. S. Barlow. Measurements of flame orientation and scalar dissipation in partially premixed methane flames. *Proc. Comb. Inst*, 30(1):665–672, 2005.

[21] R.S. Barlow, G.-H. Wang, P. Anselmo-Filho, M.S. Sweeney, and S. Hochgreb. Application of Raman/Rayleigh/LIF diagnostics in turbulent stratified flames. *Proc. Comb. Inst*, 32(1): 945 – 953, 2009.

[22] M. J. Dunn and R. S. Barlow. A wavelet based denoising algorithm optimized for high resolution line imaging in fluid mechanics. *Exp. Fluids*, 2011. Submitted.

[23] RW Bilger, SH Stårner, and RJ Kee. On reduced mechanisms for methane—air combustion in nonpremixed flames. *Comb. Flame*, 80(2):135–149, 1990.

[24] Sandia National Laboratories. Chemkin. Online, 2011. http://www.ca.sandia.gov/chemkin/.

[25] G. P. Smith and D. M. Golden. GRI-Mech 3.0. Online, 2010. URL `http://www.me.berkeley.edu/gri_mech/`.

[26] R.S. Barlow, M.J. Dunn, M.S. Sweeney, and S. Hochgreb. Effects of preferential transport in turbulent bluff-body-stabilized lean premixed ch4/air flames. *Comb. Flame*, Submitted, 2011.